microbial biotechnology

Open Access

Redirection of acyl donor metabolic flux for lipopeptide A40926B0 biosynthesis

Tian-Yu Xia,[1,2,†] Xin-Ai Chen,[1,2,†] Yan-Qiu Liu,[1,2] Daniel H. Scharf,[1,2] Qing-Wei Zhao[1] and Yong-Quan Li[1,2,*]

[1]*First Affiliated Hospital and Institute of Pharmaceutical Biotechnology, Zhejiang University School of Medicine, Hangzhou, 310058, China.*

[2]*Zhejiang Provincial Key Laboratory for Microbial Biochemistry and Metabolic Engineering, Hangzhou, 310058, China.*

Summary

The metabolic flux of fatty acyl-CoAs determines lipopeptide biosynthesis efficiency, because acyl donor competition often occurs from polyketide biosynthesis and homologous pathways. We used A40926B0 as a model to investigate this mechanism. The lipopeptide A40926B0 with a fatty acyl group is the active precursor of dalbavancin, which is considered as a new lipoglycopeptide antibiotic. The biosynthetic pathway of fatty acyl-CoAs in the A40926B0 producer *Nonomuraea gerenzanensis* L70 was efficiently engineered using endogenous replicon CRISPR (erCRISPR). A polyketide pathway and straight-chain fatty acid biosynthesis were identified as major competitors in the malonyl-CoA pool. Therefore, we modified both pathways to concentrate acyl donors for the production of the desired compound. Combined with multiple engineering approaches, including blockage of an acetylation side reaction, overexpression of acetyl-CoA carboxylase, duplication of the *dbv* gene cluster and optimization of the fermentation parameters, the final strain produced 702.4 mg l^{-1} of A40926B0, a 2.66-fold increase, and the ratio was increased from 36.2% to 81.5%. Additionally, an efficient erCRISPR-Cas9 editing system based on an endogenous replicon was specifically developed for L70, which increased conjugation efficiency by 660% and gene-editing efficiency was up to 90%. Our strategy of redirecting acyl donor metabolic flux can be widely adopted for the metabolic engineering of lipopeptide biosynthesis.

Introduction

Actinomycetes have proven to contribute various clinically applicable antibiotics. However, in the process of switching from primary to secondary metabolism, competition often occurs because different pathways may share the available precursors and energy in the host (Wan *et al.*, 2015; Lu *et al.*, 2016). Therefore, the rational redistribution of key precursors plays an important role in the efficient biosynthesis of the target product.

Lipopeptides are an important class of non-ribosomal peptide family compounds with a lipophilic acyl chain attached to the peptide core (Strieker and Dr, 2010). The fatty acyl side-chain in lipopeptides assists in dimer formation, membrane anchoring and stabilizing interactions with lipid II. These events enhance target site binding, prolong the half-life, and improve biological activity against gram-positive organisms (Zhanel *et al.*, 2010). However, congeners differing in the fatty acyl side-chain have different efficacies, which hampers the industrialization of many microbial drugs (Zerilli *et al.*, 2010; Alt *et al.*, 2019).

Fatty acid biosynthesis is an essential metabolic pathway mediated by fatty acid synthase (FAS). This biosynthesis shares similar building blocks and catalysis mechanisms with polyketide biosynthesis in microorganisms (Hopwood and Sherman, 1990). In addition, a series of acetyl coenzyme A (acyl-CoA) molecules are considered to be the common precursor in both systems. Short-chain acyl-CoA precursors, such as acetyl-CoA and isobutyl-CoA, are typically used as a starter unit in fatty acid biosynthesis, while malonyl-CoA functions as an extender unit for a growing acyl chain (Galina *et al.*, 2002; Hertweck, 2009). Many studies have focused on increasing the supply flux of acyl-CoAs into the fatty acid pathway to stimulate the production of polyketides (Li *et al.*, 2020; Ng *et al.*, 2021). However, few studies have addressed redirecting the

Received 28 September, 2021; revised 13 February, 2022; accepted 13 February, 2022.
*For correspondence. E-mail: lyq@zju.edu.cn; Tel. 86 571 88206632; Fax 86 571 88206632.
†These authors contributed equally to this work.
Microbial Biotechnology (2022) **15**(6), 1852–1866
doi:10.1111/1751-7915.14021
Funding information
This work was supported by the National Key Research and Development Program (grant number 2019YFA09005400) and key project from the National Natural Science Foundation of China (grant number 31730002).

flux of acyl donors for lipopeptide biosynthesis (Shuai *et al*., 2018, Wu et al., 2018).

Dalbavancin is a new generation antibiotic for the treatment of severe infections, including those caused by vancomycin-resistant bacteria (Boucher *et al*., 2014). Lipopeptide A40926, the precursor of dalbavancin, is a mixture of compounds differing in the fatty acyl side-chain. According to the approval requirements for dalbavancin of the Food and Drug Administration, component B0 with an isododecanol side-chain accounts for >75% of the whole complex (Cavaleri *et al*., 2005). However, due to the broad substrate specificity of the acyltransferase Dbv8, a variety of A40926B0 analogues are produced during fermentation. Previous studies showed that supplementation with L-valine could increase the production of component B0 by 1-fold from approximately 4 to approximately 8 mg l^{-1} (Jovetic *et al*., 2008). However, improving the biosynthetic efficiency of A40926B0 remains a key problem in industrial production.

Rare actinomycetes are generally not very accessible for genetic manipulation. This is a serious obstacle for further improvement of industrial strains. In *Nonomuraea gerenzanensis* L70, several genetic tools have been used for gene-editing. Among them, PCR targeting is time-consuming and incapable of achieving traceless mutagenesis (Yi *et al*., 2010). Cre/LoxP recombination is even more tedious as two rounds of conjugation are necessary (Xi *et al*., 2016). Homologous recombination (HR) with low recombination efficiency results in difficult conjugation transfer and necessary double crossover screening. In addition, the most popular gene-editing tool, CRISPR-Cas9, seemed to be useless in strain L70, since no transformants could be observed through conjugation. Therefore, efficient genetic tools are urgently required for this industrial strain.

In this study, we redirected acyl donor metabolic flux towards A40926B0 biosynthesis based on the developed endogenous replicon CRISPR (erCRISPR) system (Fig. 1). Firstly, a type Ⅱ polyketide pathway was knocked out to channel the malonyl-CoA flux for lipopeptide biosynthesis. Secondly, the production of malonyl-CoA from acetyl-CoA was enhanced by overexpression of acetyl-CoA carboxylase (ACC). Thirdly, the branched-chain α-keto acid dehydrogenase (BCDH) complex encoded by *bkdA2B2C2* was also overexpressed to further compete for malonyl-CoA between branched-chain fatty acid (BCFA) and straight-chain fatty acid (SCFA) biosynthesis. After eliminating the multilevel competition for malonyl-CoA, we introduced two extra copies of the *dbv* gene cluster. Finally, we successfully constructed a high-producing strain for A40926B0 named *N. gerenzanensis* IPB-9.

Results

Mining of the endogenous replicon in an indigenous plasmid-deficient strain

The industrial strain *N. gerenzanensis* L70 was obtained from *Nonomuraea* sp. ATCC 39727 by UV-induced mutation. Fermentation analysis showed that the yield of A40926B0 in L70 was 49.0% higher than that in the original strain (Fig. S1). Therefore, L70 was chosen for study to produce a higher yield of A40926B0. In our previous research, traditional genetic tools were shown to work with low efficiency (Fig. S2). After unsuccessfully testing several wide-host-range replicons, we focused on the mining of a suitable replicon in this industrial strain.

Two independent and stable indigenous plasmids (P1 and P2) were detected with sizes of 48321 bp and 7713 bp respectively. Genome annotation revealed 12 putative genes in P2 and 55 in P1 (Fig. 2A and Tables S1, S2). Among the 12 annotated genes in P2, *orf0012* encodes the partition A protein (ParA). ParA has ATPase activity that provides energy for plasmid partitioning (Ebersbach and Gerdes, 2005). We then investigated the endogenous replicon in the P2 deletion strain. Many methods have been developed for plasmid elimination, including high temperature, the addition of chemical reagents and the use of transposons. The deletion efficiency usually appears to be extremely low, and injuries may occur in the host (Imre *et al*., 2006; Leavitt *et al*., 2010; Zaman *et al*., 2011). Therefore, a self-targeting CRISPR-Cas9 system was designed, in which the key gene *parA* was used as the target for disruption (Fig. 2B).

We firstly engineered the CRISPR-Cas9 system based on the suicide plasmid pSET153. The *parA* gene was ligated to the vector, ensuring its survival only through integration into P2 via HR. The single guide RNA (sgRNA) expression cassette targeting *parA* and codon-optimized Cas9 from *Streptococcus pyogenes* was added to generate pSC01. The expression of Cas9 was controlled by a double-induced system comprising the thiostrepton-inducible promoter *tipAp* and theophylline-inducible riboswitch, which synergistically reduced Cas9 activity at the transcription and translation levels, respectively, during conjugation (Wang *et al*., 2019). The constructed plasmid was then transformed into L70. Very few transformants (1.5 colonies per plate) integrated into P2 naturally. Induction was later performed in which the Cas9 protein cut the DNA, leading to two cleavages, as shown in Fig. 2B. Replica plating revealed that 60% of 30 single colonies were sensitive to apramycin (Fig. S3). This involved the loss of P2 as subsequently confirmed by diagnostic PCR (Fig. 2C). To our knowledge, this is the first study to use the self-targeting CRISPR-Cas9 strategy for indigenous plasmid elimination, which is

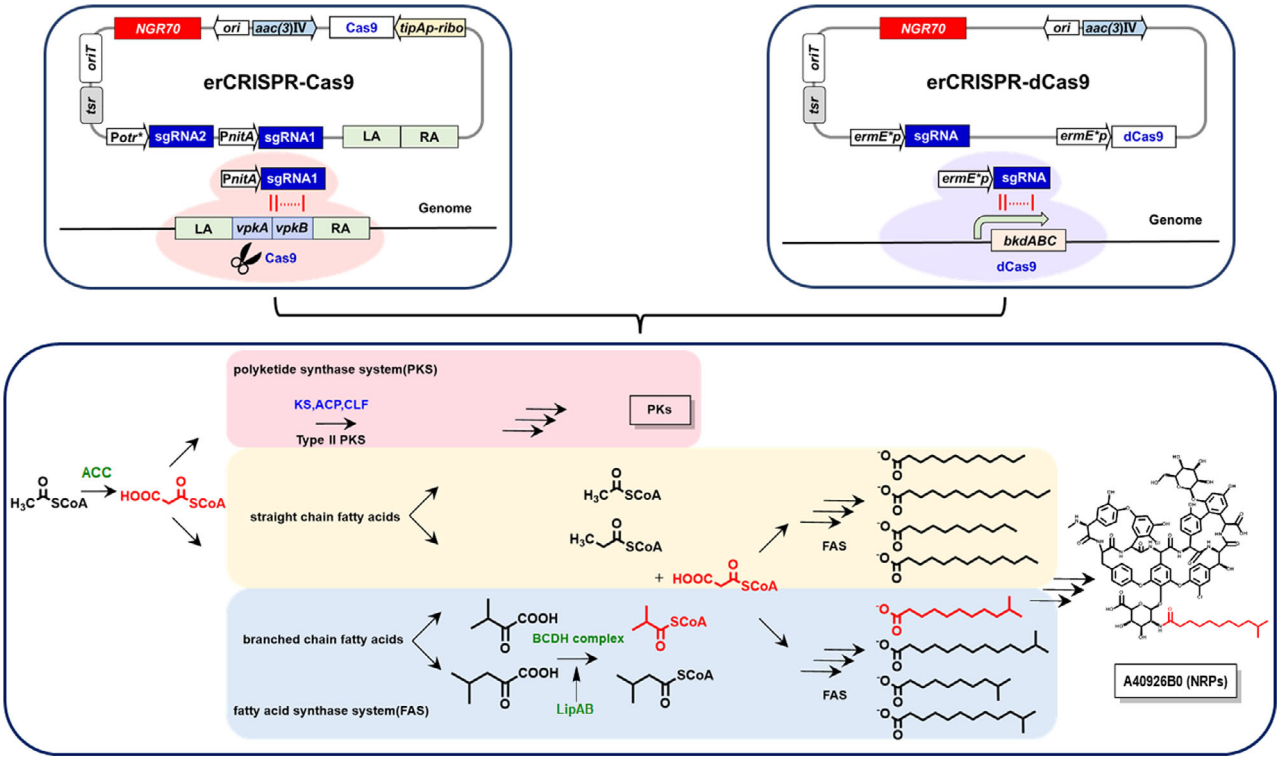

Fig. 1. Schematic diagram of redirection of acyl donor metabolic flux to A40926B0 biosynthesis based on the erCRISPR system in *Nonomuraea gerenzanensis* L70. The engineering strategies include blockage of the competing pathway (shown in blue), overexpression of critical enzyme (shown in green) and enhancement of specific precursor (shown in red). Abbreviations are: ACC, acetyl-CoA carboxylase; ACP, acyl carrier protein; BCDH complex, branched-chain α-keto acid dehydrogenase complex; CLF, chain length factor; KS, ketosynthase; LipAB, lipoyl synthase & lipoyl transferase; NRPs, non-ribosomal peptides; PKs, polyketides.

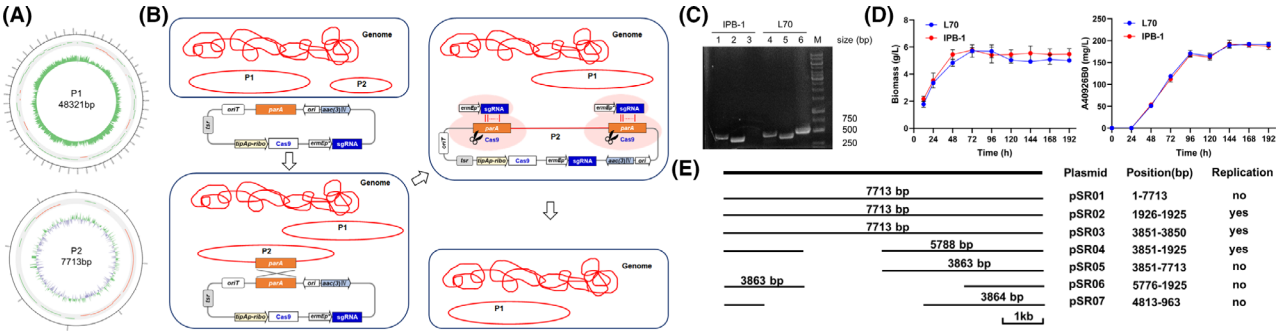

Fig. 2. Mining of the endogenous replicon NGR70 in *Nonomuraea gerenzanensis*.
A. Plasmid maps of P1 and P2 from *N. gerenzanensis* L70. Circle 1 displays the predicted ORFs. Circle 2 displays the GC skew (±).
B. Overview of the self-targeting CRISPR-Cas9 strategy for P2 deletion in *N. gerenzanensis* L70.
C. Identification of ΔP2 mutant by diagnostic PCR. Lane 1 and 4 show PCR products amplified by genome-F/genome-R primer pairs. Lane 2 and 5 show PCR products amplified by P1-F/P1-R primer pairs. Lane 3 and 6 show PCR products amplified by P2-F/P2-R primer pairs.
D. Effect of P2 deletion on cell growth and A40926B0 production. Dry weight of mycelia was measured in the wild-type strain (L70) and the P2 deletion strain (IPB-1) at different incubation times as shown. A40926B0 production of L70 and IPB-1 at different incubation times as shown. Standard deviation (SD) bars are shown.
E. Identification of the replication region of P2. A linear map of P2 is shown at the top. The bars below the map representing P2 regions covered in the respective plasmids.

highly efficient and host-friendly. No significant difference was observed between the P2 deletion strain IPB-1 and L70 in biomass and A40926B0 production, indicating that P2 might have no critical effect (Fig. 2D).

The minimal replication region of P2 was further determined in IPB-1. The vectors pSR01–pSR07 with different regions of P2 were independently introduced into IPB-1. Transformants were observed with vectors

pSR02, pSR03 and pSR04, whereas no transformants grew out using the other vectors (Fig. 2E). The essential region for P2 self-replication consisted of a 5788 bp fragment (named NGR70) with eight open reading frames (ORFs). Sequence alignment indicated that NGR70 is a new replicon in actinomycetes (Fig. S4). Furthermore, NGR70 is the first replicon available in *N. gerenzanensis*, with the potential for development into a powerful genetic tool.

Construction of a sequential gene targeting erCRISPR-Cas9 system

To broaden the application of the self-targeting CRISPR-Cas9 system, we combined it with NGR70 for genetic manipulation. The *tipAp* promoter and riboswitch were introduced into vector pSR04 to control the expression of Cas9. Two sgRNA expression cassettes were controlled by two independent inducible promoters, P*nitA* and Potr*, which respectively targeted the specific gene and the *parA* gene of the vector (Herai *et al*., 2004; Wang *et al*., 2016). Finally, one pair of homologous flanking regions of the specific gene with 3.0 kb was introduced into the vector (Fig. 3B), which functioned as the template for repairing the double-strand break mediated by Cas9.

Based on the above steps, we constructed the all-in-one vector pSRK04 for the traceless deletion of the ketosynthase (*KS*) gene named *vpkAB* (Fig. 3A). Through conjugation based on erCRISPR-Cas9, approximately 24 positive transformants were obtained on each plate. The efficiency was 2.87-fold higher than that mediated by the suicide vector pSK03 with the same homologous arms (Fig. 3E). Then, we transferred three transformants to the YEME liquid culture for 16 h at 28°C. The sgRNA cassette and Cas9 protein were induced for 48 h by supplementing with 5 μM thiostrepton, 8 mM theophylline and 15 mM ε-caprolactam to delete the *vpkAB* gene. Gene-editing efficiency was evaluated using PCR analysis and sequencing (Fig. 3C and 3D). Nearly 90% (86/96) of the colonies were identified as Δ*vpkAB* mutants, which was nearly 20-fold higher than that of the traditional HR strategy (4.2%, 4/96) based on pSK03 (Fig. 3E).

The second round of induction was performed to eliminate the plasmid itself in these mutants. 5 μM thiostrepton, 8 mM theophylline and 6 μM oxytetracycline were added to switch on the transcription of the *parA*-sgRNA cassette along with the Cas9 protein when the mycelia were cultured in YEME for 16 h. After a 48-h incubation, the transformants were transferred to a YMG solid plate for successive subculture. Diagnostic PCR revealed that all 30 transformants lost the plasmid because of the continuous cutting by Cas9 and the absence of a corresponding repair template (Fig. S5). The mode of traceless deletion ensures multiple usages of the erCRISPR-Cas9 system. Moreover, the time for gene-editing was greatly shortened from 52 d to 32 d, as the traditional editing method relying on HR requires multiple subcultures to obtain mutant colonies (Table 1).

Blocking polyketide synthesis to redistribute the metabolic flux of malonyl-CoA

N. gerenzanensis L70 is known for producing A40926B0, the precursor of dalbavancin. To improve the yield of A40926B0, we first constructed the IPB-2 strain by deleting the *dbv23* gene, which encodes a pathway-specific acetyltransferase responsible for acetylating the mannose moiety of A40926B0 (Sosio *et al*., 2010). Liquid chromatography-mass spectrometry (LC-MS) analysis showed that the A40926B0 yield was up to 251.6 mg l^{-1} and eight components differing in the fatty acyl chain were detected in fermentation broths (Fig. 4A, B, S6 and S7). These moieties consisted of a straight-chain or branched-chain fatty acyl group with 11 to 14 carbon atoms. The A40926 complex composition has been closely related to the cell fatty acid pattern (Jovetic *et al*., 2008). Thus, we speculated that the composition of A40926 could be affected by changing the content of related fatty acids in the strain.

So far, the non-ribosomal peptide A40926, encoded by 37 ORFs, is the only secondary metabolite reported in *N. gerenzanensis* (Sosio *et al*., 2003). RNA-seq analysis also showed that many other gene clusters were in a cryptic state or low-level expression, except for a type II PKS-encoding cluster (cluster 23), designated here as the *vpk*-gene cluster (Fig. 5A, 5B and Table S3). The expression of the core synthase gene *vpkAB* in the *vpk*-gene cluster (Table S4) was detected at a relatively high level. Since malonyl-CoA is used as the common extender unit in the biosynthesis of type Ⅱ polyketide and fatty acids, we sought to redistribute the metabolic flux of malonyl-CoA into A40926 biosynthesis by blocking the polyketide pathway (Fig. 4C).

The vector pSRK04 for in-frame deletion of the *vpkAB* gene was transformed into IPB-2, mediated by the developed erCRISPR-Cas9 system to generate IPB-3. Compared with the parent strain, the pigment production of IPB-3 was significantly reduced in shaker fermentation (Fig. 5C). High-performance liquid chromatography (HPLC) analysis also demonstrated that IPB-3 possessed cleaner metabolite profiles than IPB-2, indicating the elimination of the pigment compounds produced by the *vpk*-gene cluster (Fig. 5D). The metabolites related to primary metabolic pathways, including the tricarboxylic acid cycle, pentose phosphate pathway, Embden-Meyerhof-Parnas pathway, amino acid metabolism and

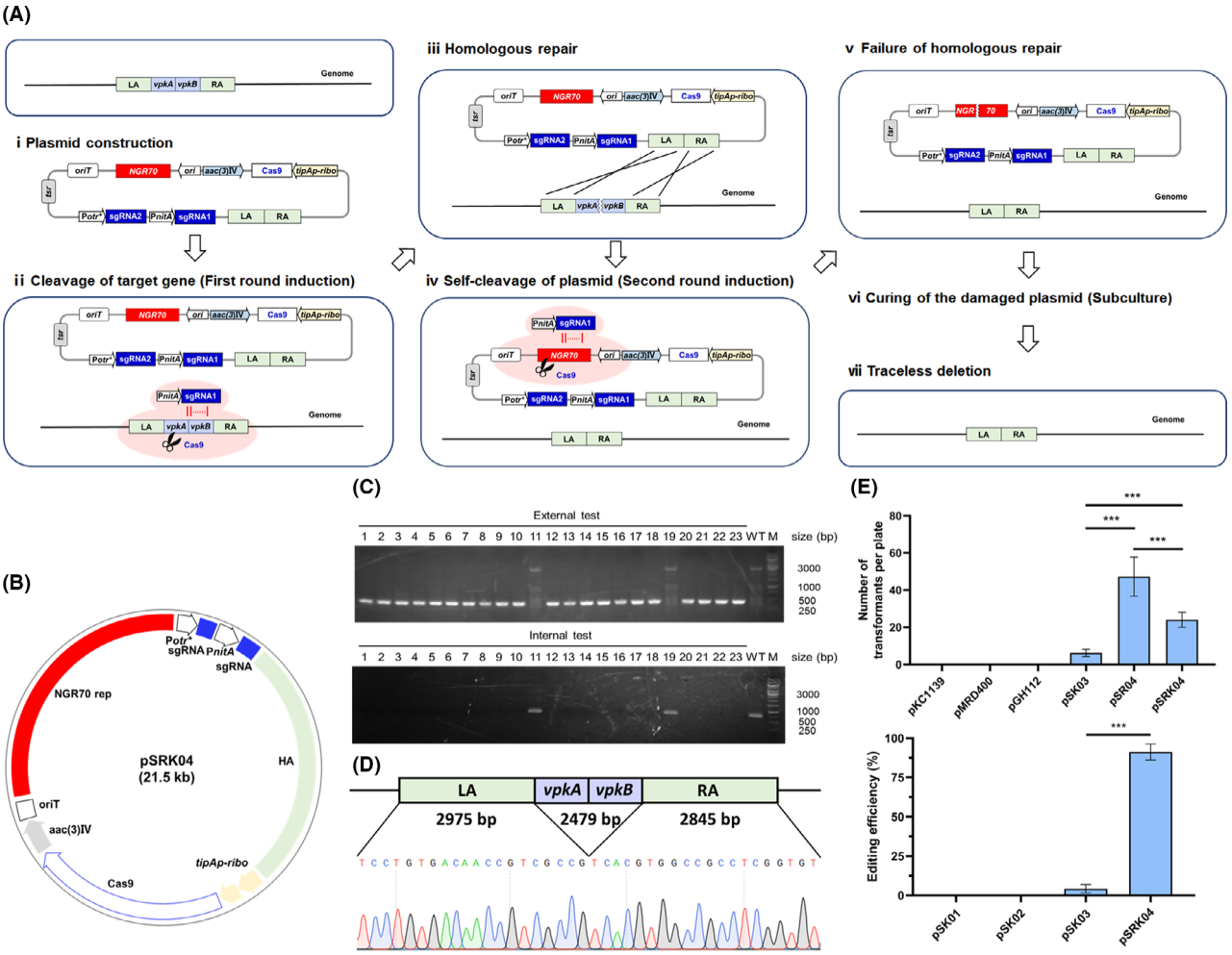

Fig. 3. Establishment of a sequential gene targeting erCRISPR-Cas9 system in *Nonomuraea gerenzanensis*.
A. Schematic overview of the sequential gene targeting erCRISPR-Cas9 strategy for *vpkAB* deletion in *N. gerenzanensis*.
B. Plasmid map of pSRK04 for *vpkAB* deletion based on the erCRISPR-Cas9 system. All the genetic cassettes are labelled as shown.
C. Diagnostic PCR results of Δ*vpkAB* mutant. The external test used vpkABexternal-F/R primer pairs. The internal test used vpkABinternal-F/R primer pairs.
D. DNA sequencing analysis of Δ*vpkAB* mutant.
E. Evaluation of the conjugation efficiency and gene-editing efficiency between different plasmid tools. Significant statistical differences are shown (***$P < 0.001$). SD bars are also shown

lipid metabolism (LPM), were identified and compared. The levels of metabolites in LPM showed a remarkable increase in IPB-3, while no significant change was detected in other pathways (Fig. 5E and S8). The yield of the A40926 components was subsequently tested by analysing the peak area from the HPLC chromatogram. No significant difference was observed in most components, including A40926B0 (3). In contrast, A40926B1 (4), with a straight-chain decanoyl group, was significantly increased in IPB-3 by 92.2% (Fig. 5F). These data indicated that deletion of the *vpkAB* gene transferred the malonyl-CoA from the PKS pathway to the FAS pathway associated with lipopeptide synthesis, favouring the biosynthesis of SCFAs instead of BCFAs. In addition, the intracellular ATP and NADH/NAD$^+$ levels were increased by nearly 2-fold in IPB-3. This might provide more cellular energy and reducing power for the improved productivity of A40926B0 in the future studies (Fig. 5G).

Enhancing metabolic flux in target fatty acid pathway

Overexpression of ACC improves the supply of malonyl-CoA. Since blockage of the *vpk*-gene cluster biosynthetic pathway resulted in a redistribution of malonyl-CoA flux into fatty acid biosynthesis, the next

Table 1. Efficiency comparison between erCRISPR-Cas9 system and the traditional genetic tool based on HR used in *Nonomuraea gerenzanensis*.

erCRISPR-Cas9		HR by suicide vector	
Plasmid construction	9 days	Plasmid construction	7 days
Conjugation	9 days	Conjugation	9 days
Subculture	4 days	Subculture	4 days
First induction gene-editing	5 days	Double crossover screening	4 days* 8 = 32 days
Second induction plasmid elimination	5 days		
Total	32 days	Total	52 days
Conjugation efficiency[a]	24	Conjugation efficiency[a]	6.2
Editing efficiency	90.9%	Editing efficiency	4.2%

a. Conjugation efficiency was calculated as the number of positive transformants obtained on each plate.

step was to increase the malonyl-CoA pool to improve precursor supply.

In actinomycetes, the ACC complex catalyses the conversion of acetyl-CoA to malonyl-CoA and is composed of three subunits that perform different functions. The activity of ACCase affects the efficiency of fatty acid synthesis (Koendjbiharie, 2015, Satoh et al., 2020). We cloned the genes *accA*, *accB and accC* together in an integrative vector under the control of the *ermE** promoter and transformed the vector in IPB-3 to obtain IPB-4. The peak area of A40926B1 (4) increased by 132.0% and 20.7%, respectively, compared with those of IPB-2 and IPB-3, while no significant changes were observed in other components (Fig. S9).

Identifying the pivotal bkd cluster to enhance the precursors in BCFA synthesis. In the biosynthetic pathway of SCFAs, the main initial unit of acetyl-CoA is relatively abundant, as it plays an essential role in primary metabolism. To further enhance the production of A40926B0 with a branched-chain isododecanoyl group, the key bottleneck was to improve the biosynthesis of BCFAs, which may compete for malonyl-CoA with SCFAs. In contrast, isobutyryl-CoA and isovaleryl-CoA, which function as specific precursors of BCFAs, were reported to be only derived from branched-chain amino acid (BCAA) degradation.

In BCFA catabolism, a *bkd* gene cluster containing *bkdA/B/C* genes encodes the subunits E1α, E1β and E2 of the branched-chain α-keto acid dehydrogenase complex (BCDH complex). The BCDH complex catalyses the oxidative decarboxylation of α-keto acids derived from BCAAs to produce the corresponding acyl-CoA derivatives, which then act as precursors for BCFA biosynthesis (Stirrett *et al.*, 2009).

As reported in other streptomyces (Stirrett *et al.*, 2009; Shuai *et al.*, 2018), two alleles of *bkd* gene clusters were located in L70 through BLAST alignment (Fig. 6A and S10). To investigate their functions in this industrial strain, the vectors pSRB01 and pSRB02, which include sgRNA targeting the promoter of the corresponding *bkd* cluster along with the dCas9 protein, were transformed into IPB-4 (Fig. S11). Transcriptional analysis revealed a significant decrease in the expression levels of

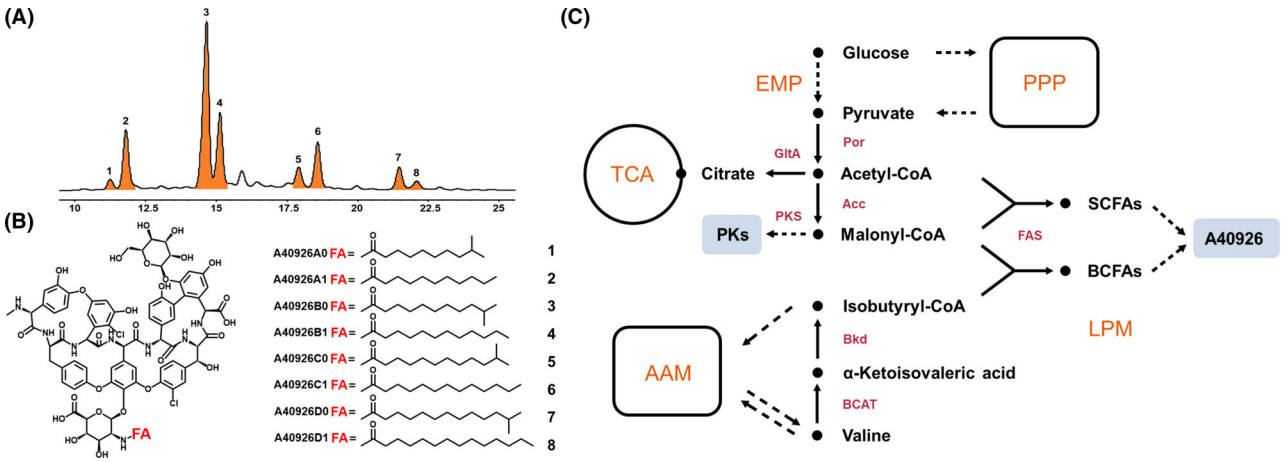

Fig. 4. A40926 complex and its related fatty acyl side-chain.
A. HPLC analysis of A40926 components in fermentation extracts of *Nonomuraea gerenzanensis* L70. The numbered peaks represent eight components of A40926 that were confirmed by LC-MS data and ultraviolet (UV) absorption as shown in Fig. S6.
B. Chemical structures of A40926 complex. The acyl group was shown as FA (fatty acyl). Structures of FA moieties in the A40926 complex are shown with the corresponding marked numbers in HPLC analysis.
C. Partial metabolic pathway in *N. gerenzanensis* L70. Solid arrow denotes the direct reaction and the dotted arrow denotes the indirect reaction.

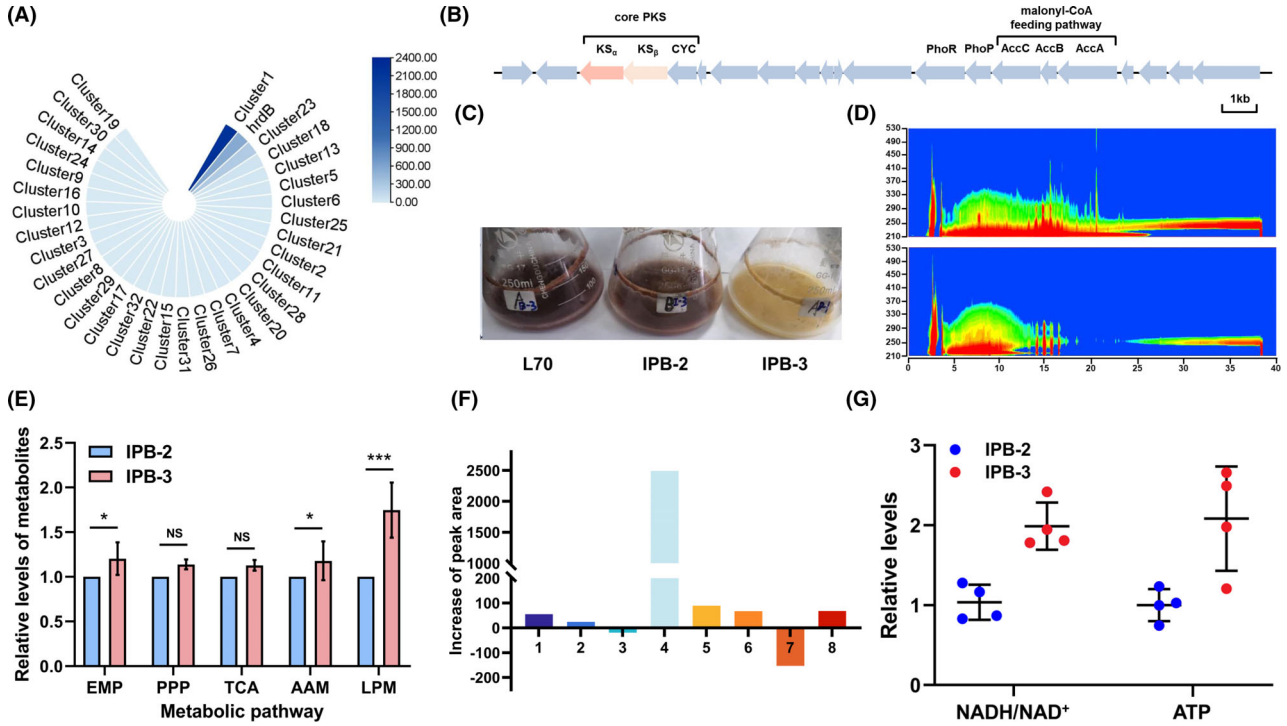

Fig. 5. Blockage of the *vpk*-gene cluster biosynthetic pathway results in redistribution of malonyl-CoA flux.
A. Analysis of relative expression levels of putative gene clusters in *Nonomuraea gerenzanensis* L70 based on RNA sequencing data. The housekeeping gene *hrdB* was chosen as the reference gene.
B. Genetic organization of the *vpk*-gene cluster in *N. gerenzanensis* L70.
C. Phenotypic appearance of culture broths of wild-type and mutant strains after cultivation for 168 h in YS medium.
D. Comparison of metabolite profiles analysis based on isoabsorbance plot between IPB-2 and IPB-3.
E. Relative levels of the identified metabolites in the different metabolic pathways in IPB-2 and IPB-3 from cultures at 36 h in YS medium. Significant statistical differences are shown (***, $P < 0.001$; **, $P < 0.01$; *, $P < 0.05$; NS, not significant). SD bars are also shown.
F. Production analysis of each component corresponding to the number of A40926 complex (Fig. 4B) by HPLC in IPB-3 compared with that in IPB-2.
G. Relative levels of intracellular NADH/NAD^+ ratio and ATP concentration in IPB-2 and IPB-3 from cultures at 36 h in YS medium. Abbreviations are: AAM, amino acid metabolism; AccA, acetyl-CoA carboxyl transferase subunit; AccB, acetyl-CoA carboxylase biotin carboxyl carrier protein; AccC, acetyl-CoA carboxylase biotin carboxylase subunit; CYC, cyclase; EMP, Embden-Meyerhof-Parnas pathway; KS_α, ketosynthase alpha subunit; KS_β, ketosynthase beta subunit; LPM, lipid metabolism; PhoP, response regulator; PhoR, sensor kinase; PPP, pentose phosphate pathway; TCA, tricarboxylic acid cycle.

bkdA1B1C1 and *bkdA2B2C2* in the respective resulting transformants IPB-5 and IPB-6 (Fig. S12). The production levels were examined. The yield of A40926B0 was reduced by 7.7% in IPB-5 and 48.4% in IPB-6 when compared with IPB-4. As a similar tendency was observed in the corresponding ratio, we surmised that *bkdA2B2C2* played a critical role in BCFA biosynthesis based on the erCRISPR-dCas9 system (Fig. 6B). On the other hand, lipoylation involving LipAB was reported to be insufficient for BCFA production (Bentley *et al.*, 2016). *bkdA2B2C2* and *lipAB* were overexpressed in IPB-4 to obtain IPB-7. Fermentation analysis showed that the A40926B0 titre in IPB-7 was improved to 342.2 mg l^{-1}, which corresponds to an increase of 36.1%, compared with that in IPB-4. Remarkably, the production of A40926 components with a straight-chain fatty acyl group in the side-chain was reduced to various degrees, among which A40926B1 showed the biggest decline of 43.1% in IPB-7 when compared with IPB-4 (Fig. 6C).

To further evaluate the effect of our rational engineering, we examined the composition of cell fatty acids based on GC-MS analysis of their methyl esters (Fig. 6D and S13). As shown in Fig. 6E and F, deletion of the *vpkAB* gene resulted in an increase in SCFAs, including n-C16:0 and n-C18:0, in IPB-3. The combinatorial strategy of strengthening the BCFA metabolic flux in IPB-7 enhanced both the amount and ratio of i-C16:0, which may act as the donor of the isododecanoyl moiety in A40926B0. These results agreed with the changes in the A40926B0 ratio and production, indicating that the metabolic flux of malonyl-CoA was redirected into the biosynthesis of the target product A40926B0 after precursor redirection. In addition, transcripts of genes

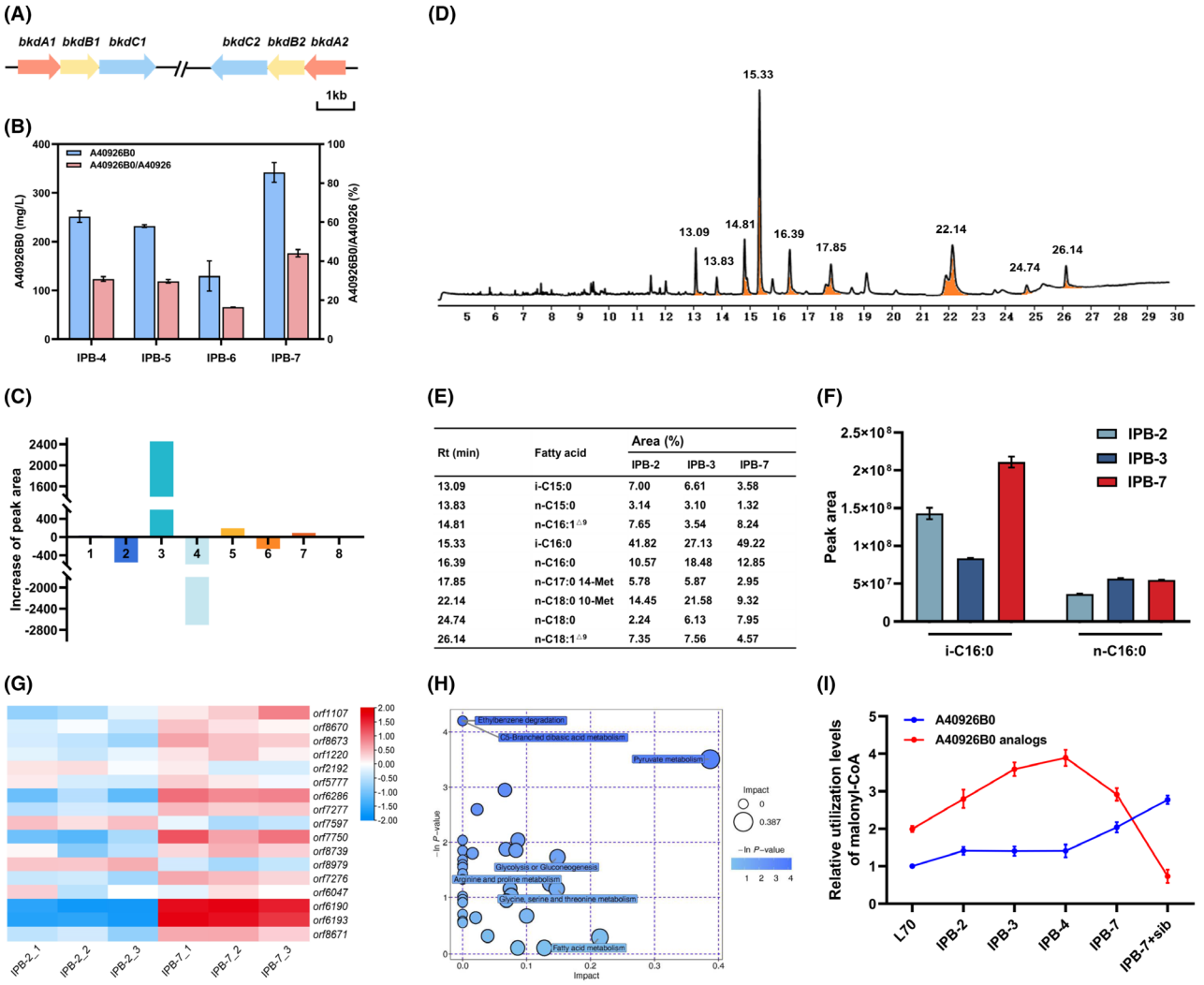

Rt (min)	Fatty acid	Area (%)		
		IPB-2	IPB-3	IPB-7
13.09	i-C15:0	7.00	6.61	3.58
13.83	n-C15:0	3.14	3.10	1.32
14.81	n-C16:1$^{\Delta 9}$	7.65	3.54	8.24
15.33	i-C16:0	41.82	27.13	49.22
16.39	n-C16:0	10.57	18.48	12.85
17.85	n-C17:0 14-Met	5.78	5.87	2.95
22.14	n-C18:0 10-Met	14.45	21.58	9.32
24.74	n-C18:0	2.24	6.13	7.95
26.14	n-C18:1$^{\Delta 9}$	7.35	7.56	4.57

Fig. 6. Identification of the pivotal *bkd* gene cluster in the BCFA biosynthetic pathway.
A. Genetic organization of two *bkd* gene clusters *bkdA1B2C1* and *bkdA2B2C2* in *Nonomuraea gerenzanensis* L70.
B. Comparison of A40926B0 production and A40926B0/A40926 ratio between IPB-4 and its engineering strains including IPB-5, IPB-6 and IPB-7 in YS medium. SD bars are shown.
C. Production analysis of each component corresponding to the number of A40926 complex (Fig. 4B) by HPLC in IPB-7 compared with that in IPB-4.
D. GC-MS profiles of the FAMEs for *N. gerenzanensis* cell fatty acids from cultures at 72 h in YS medium.E. Composition analysis of fatty acids in different strains.
F. Comparison of the contents of i-C16:0 and n-C16:0 between IPB-2, IPB-3 and IPB-7.
G. Transcriptional profiles of genes involved in fatty acid biosynthesis.
H. Pathway enrichment analysis of IPB-7 vs IPB-2.
I. Relative utilization levels of malonyl-CoA by A40926B0 and its analogues in different strains.

including *fabD*, *fabF*, *fabG*, *fabI*, *fabK and fabH*, which are essential for fatty acid biosynthesis, were upregulated in IPB-7 (Fig. 6G). Similar trends were observed in the metabolome analysis, which revealed that metabolites associated with fatty acid metabolism showed relatively large differences between IPB-7 and IPB-2. Furthermore, the abundance of metabolites in pyruvate metabolism also exhibited otherness, possibly because pyruvate, as a central metabolic hub, is susceptible to the engineering of other metabolic pathways (Fig. 6H). In general, through our redirection research strategy, fatty acid metabolism, especially the branched-chain one, tended to be more active, which could provide sufficient precursor supply for the efficient biosynthesis of A40926B0.

Further improvement in the composition of A40926B0 by supplying sodium isobutyrate. Given that enhancement

of specific precursors could reduce homologues by competing for malonyl-CoA donors, we attempted to further improve the precursor supply through exogenous addition. The effect of sodium isobutyrate on A40926B0 production was subsequently examined by culturing IPB-7 in YS medium (Fig. S14). 10 mM of sodium isobutyrate was found to be the optimal concentration to achieve the highest yield of 448.2 mg l^{-1}. By supplying sodium isobutyrate to IPB-7, A40926B0 was increased remarkably by 31.0%, while A40926B1 was decreased by 52.1%, compared with that in IPB-7 (Fig. S15). Moreover, calculation of the relative utilization levels of malonyl-CoA revealed a 177.5% increase for A40926B0 together with a 63.2% decrease for other analogues (Fig. 6I). The interaction between Dbv8, the key gene for generating congeners, and different fatty acyl-CoA molecules was analysed by affinity calculation through molecular docking (Lyu *et al.*, 2014). Isododencanoyl-CoA exhibited the strongest binding affinity towards the Dbv8 protein, which explains why sodium isobutyrate supplementation increased A40926B0, rather than A40926D0 (7), although they shared the same precursor isobutyryl-CoA (Fig. S16).

Construction of a higher A40926B0-producing strain by cluster duplication and fermentation optimization

Duplication of gene clusters has been reported to effectively improve the titre of target compounds (Li *et al.*, 2017). Here, the vector pMSBBAC1 containing a complete *dbv* gene cluster was screened from the bacterial artificial chromosome library and introduced into IPB-3 along with pSOA02 containing the overexpression cassettes of *accABC*, *bkdA2B2C2 and lipAB*. A further increase of 58.5% was observed in A40926B0 production (Fig. 7B). Based on these results, we attempted to increase the copy number of pMSBBAC1. An artificial ΦC31 *attB* site was introduced into the chromosome of IPB-3 by replacing the synthase gene of a putative terpene gene cluster (cluster 32) via erCRISPR-Cas9 (Fig. 7A). The vectors pMSBBAC1 and pSOA02 were successively transformed into the parental strain to obtain IPB-9, which contains two extra copies of the *dbv* gene cluster (Fig. S17). Production analysis revealed that IPB-9 produced A40926B0 at a titre of 507.3 mg l^{-1}, which was nearly 48.2% and 164.2% higher than that of IPB-6 and L70 respectively (Fig. 7B).

Scale-up fermentation was further performed to verify the production of A40926B0 by IPB-9 in a 2-L flask with 350 ml working volume in YS medium supplemented with 10mM sodium isobutyrate. After culturing for 168 h, the titre of A40926B0 reached 550.8 mg l^{-1}, with the productivity of 0.43 mg g^{-1} dry cell weight h^{-1} (Fig. 7B and C). The time course profile showed that production of A40926B0 increased continuously from 48 h to 96 h and reached a plateau after culturing for 120 h and 48 h earlier than that of the wild-type strain (Fig. 7D). Therefore, sodium isobutyrate was fed at a rate of 10 mM for 24 h

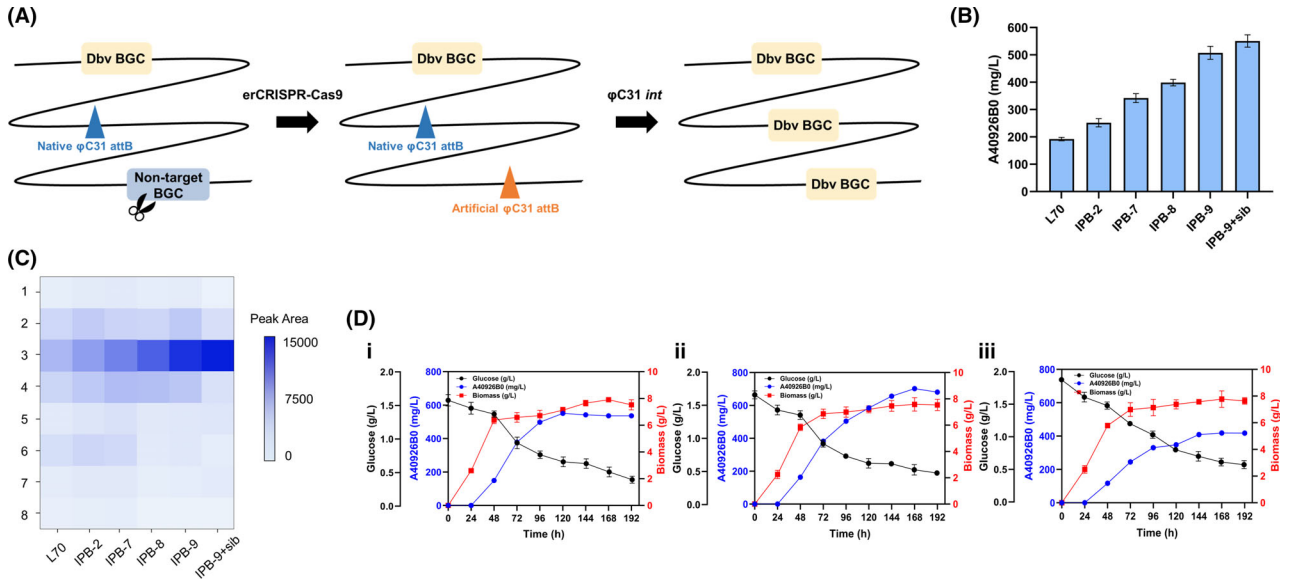

Fig. 7. Further improvement of A40926B0 production.
A. Diagram of the introduction of *dbv* gene clusters in the parental strain.
B. A40926B0 production in the engineering strains. SD bars are shown.
C. Heat map of the peak area of the A40926 components in different strains. The numbers of components correspond to those in Fig. 4B.
D. Time-course profile of A40926B0 fermentation. IPB-9 strain in YS medium with 10 mM sodium isobutyrate (i), IPB-9 strain in YS medium with continuous feeding of 10 mM sodium isobutyrate (ii), L70 strain in YS medium with continuous feeding of 10 mM sodium isobutyrate (iii). Fermentation broths were sampled for analysis every 24 h. SD bars are shown.

from 96 h to relieve the precursor deficiency, leading to a higher titre of 702.4 mg l^{-1} of A40926B0 at 168 h (Fig. 7D), which increased the proportion from 36.2% to 81.5% (Fig. S18). This is the highest A40926B0 titre in *N. gerenzanensis* reported to date. Given the excellent potential of this genetically engineered strain, the productivity of *N. gerenzanensis* IPB-9 may be further improved through bioprocess optimization in a bioreactor.

Discussion

Malonyl-CoA is an important central metabolite that serves as the elongation unit for the biosynthesis of polyketides and the acyl chain of lipopeptides. Commonly, intracellular malonyl-CoA availability is regarded as a crucial bottleneck limiting target product formation (Milke and Marienhagen, 2020). Several strategies have been adopted to boost polyketide production by improving the supply of malonyl-CoA, such as enhancement of ACC activity and inhibition of fatty acid or by-product polyketide synthesis (Santos *et al*., 2011; Zabala *et al*., 2013; Kallscheuer *et al*., 2016). However, few studies have focused on the flux of malonyl-CoA for lipopeptide biosynthesis. One typical example is the production of surfactin was improved with a higher level of malonyl-ACP through overexpression of ACC and FabD (Wu et al., 2018). Fatty acids play important roles in growth maintenance and secondary metabolite production, which makes the precise control of malonyl-CoA metabolic flux challenging. In this study, the key synthase enzyme of a major polyketide by-product was deleted to channel the malonyl-CoA flux to the lipopeptide A40926 biosynthesis, which represents the first example of channelling the key precursor malonyl-CoA from polyketide biosynthesis into lipopeptide biosynthesis.

In A40926 biosynthesis, a series of congeners mainly derived from the degradation of cellular SCFAs were produced. However, the biosynthesis of SCFAs seems difficult to block because the end product palmitic acid is essential for the growth and is derived from acetyl-CoA. However, the initial substrate of BCFA biosynthesis is typically controlled by the *bkd* cluster. Considering that A40926B0 has a branched-chain isododecanoyl group, it seems feasible to compete for malonyl-CoA from the SCFA pathway by regulating *bkd* cluster expression. *bkdA2B2C2* overexpression significantly improved the A40926B0 titre, together with a reduction in by-product production. The yield of A40926B0 was further increased by the addition of sodium isobutyrate. As the feedstock precursor, sodium isobutyrate could be obtained through an equal-molar chemical reaction of isobutyric acid and sodium hydroxide, which enabled the efficient utilization of malonyl-CoA from the fatty acyl pathway in A40926B0 production. A remarkable increase in the A40926B0 titre was achieved based on our strategy, suggesting that insufficient supply of acyl precursors is a key obstacle for A40926B0 production. Besides, the replacement of promoter in the above overexpression cassettes and the increase of *dbv* gene cluster copy number are expected to enhance the A40926B0 yield further. Overall, our work provides an efficient strategy for reducing the metabolic flux in branching pathways by competing for common precursors, which can be applied to improve the amount of target product in the mixture through rational metabolic engineering.

An efficient genetic manipulation system is a prerequisite for remodelling industrial microorganisms. Efforts to enhance conjugation efficiency have included improving the DNA uptake by the recipient strain via protoplast preparation (Marcone *et al*., 2010), sonication (Sofia *et al*., 2010), electroporation (Cho *et al*., 2017) and optimization of the culture conditions, including concentrations of Mg^{2+} and Ca^{2+} (Wang and Jin, 2014), temperature and medium (Netzker *et al*., 2016). However, these explorations have been time-consuming and labour-intensive. In *N. gerenzanensis* L70, we optimized the conjugation efficiency from all aspects and found that many transformants could be obtained by integrative vector-mediated conjugation. Nevertheless, these attempts seem to be useless for episomal vectors. We hypothesize that the incompatibility of replicons might be the key factors affecting conjugation efficiency. Replicons in endogenous plasmids have been developed in *Propionibacterium*, *Pseudomonas alcaligenes* and other microorganisms and have proven to be efficient for conjugation (Kwong *et al*., 2000, Kiatpapan and Murooka, 2002). However, no studies have reported the coupling of endogenous replicons with the CRISPR system. Here, by identifying the endogenous replicon NGR70, we developed an inducible erCRISPR-Cas9 system for traceless mutagenesis. The presence of NGR70 ensured the replication of the plasmid, and increased Cas9 and sgRNA expression levels in the host. The efficiency of conjugation and gene-editing was improved by 6.6-fold and 22-fold respectively. Thus, we conclude that replicon adaptability may be the key for genetic manipulation of many industrial strains. Interestingly, NGR70 had no homology with known replicons, and it may further be developed into an element for universal vectors with potential applications in other actinomycetes. In brief, our work provides a novel genetic strategy based on the examination of replicon compatibility with the host, which will be universally applicable to industrial strains.

Overall, a combinatorial approach was used to concentrate the metabolic flux of acyl donors into the biosynthetic route of the fatty acyl side-chain in A40926B0 based on the developed erCRISPR system. The fermentation yield of A40926B0 is up to 702.4 mg l^{-1} in flask

increased by 2.66-fold. A40926B0 accounted for 81.5% compared to 36.2% in the original strain. Our study deciphered the metabolic flow distribution of acyl donors during drug biosynthesis in actinomycetes and provided a widely applicable strategy for the efficient biosynthesis of lipopeptides for research and industrialization.

Experimental procedures

Bacterial strains and growth conditions

The plasmids and strains used in this study are listed in Table S5. *Escherichia. coli* DH5α was used as the host for plasmid construction. *E. coli* ET12567/pUZ8002 was used as a donor for intergeneric conjugation. *E. coli* was grown at 37°C in Luria–Bertani (LB) medium (1% tryptone, 0.5% yeast extract, 1% NaCl). *N. gerenzanensis* L70 and its mutants were cultured on YMG solid medium (1% malt extract, 0.4% yeast extract, 0.4% glucose, 0.2% $CaCO_3$ and 2% agar) at 28°C for growth. For fermentation, a 1 cm^2 agar piece was incubated in a 100 ml flask with 20 ml seed medium YEME (4% glucose, 0.5% tryptone, 0.3% malt extract, 0.3% yeast extract) at 28°C with shaking at 220 rpm for 2 d. Then, 2% seed culture was transferred into a 250 ml flask with 35 ml fermentation medium YS (1% soluble starch, 0.3% malt extract, 0.2% yeast extract) at 28°C with shaking at 220 rpm for 7 d. MS solid medium (2% soya flour, 2% mannitol, 2% agar) supplemented with 10 mM $MgCl_2$ was used for interspecies conjugation between *E. coli* ET12567/pUZ8002 and *N. gerenzanensis* mycelia. If needed, antibiotics were added as follows: 50 μg ml^{-1} apramycin, 25 μg ml^{-1} chloramphenicol, 50 μg ml^{-1} kanamycin and 25 μg ml^{-1} nalidixic acid.

Design of sgRNAs from N. gerenzanensis *L70 genome and plasmid sequence*

The sgRNAcas9 software package was applied to rapidly search for CRISPR target sites (Xie *et al.*, 2014). All 20 nucleotide-NGG sgRNA sequences of the target genes in the *N. gerenzanensis* L70 genome or endogenous plasmid were selected as candidate binding sites. Programs were used to search for CRISPR target sites with user-defined parameters, and the potential off-target cleavage sites of CRISPR-Cas9 were analysed. By comparing the total number of the potential off-target sites for each CRISPR target sequence, we selected precise sgRNA candidates with high specificity. All the designed sgRNAs are listed in Table S6.

Plasmid construction

The primers used in this study are listed in Table S7. The primers were synthesized using GENEray (Shanghai, China). PCR amplification was performed using Phanta Max Super-Fidelity DNA Polymerase (Vazyme, Nanjing, China) and identification was performed using 2×Hief™ PCR Master Mix (Yeasen, Shanghai, China). A HiPure Gel Pure DNA Mini Kit (Magen, Guangzhou, China) was used to purify the PCR fragments, and the Plasmid Miniprep Kit (GENEray) was used to isolate plasmid DNA. All enzymes used for DNA manipulation were purchased from Thermo Fisher Scientific (Waltham, MA, USA). Ligation reactions were performed by seamless cloning using the ClonExpress II One Step Cloning Kit (Vazyme, Nanjing, China). The primers parA-F1/R1, cas9-F1/R1, parA-sgRNA-F1/R1 and parA-sgRNA-F2/R2 were used to amplify the *parA* gene, *tipAp* fragment and riboswitch associated with the codon-optimized Cas9, *ermE** promoter and the gRNA scaffold from vector pKC1139-TRMA, followed by ligation into the pSET153 plasmid, yielding pSC01 (Wang *et al.*, 2019). To construct pSR01–pSR07, seven fragments were amplified from genomic DNA and generated R1–R7, which covered the position 1–7713 bp, 1926–1925 bp, 3851–3850 bp, 3851–1925 bp, 3851–7713 bp, 5776–1925 bp, 4813–963 bp respectively. The R1–R7 fragments were ligated into the EcoRI and HindIII sites of pSET153 to obtain the vectors. To construct pSRK04, the primers cas9-F2/cas9-R2, vpkAB-sgRNA-F/R, parA-sgRNA-F2/R3, Potr-F/R and Pnit-F/R were used to amplify the *tipAp*-ribo-Cas9, *vpkAB*-sgRNA, *parA*-sgRNA, Potr* and P*nitA* promoters from vector pKC1139-TRMA, pIW01 and pL99. (Sun *et al.*, 2012; Wang *et al.*, 2016). Finally, the 3.0 kb homologous arms flanking the *vpkAB* gene were amplified from genomic DNA and ligated into the Eco105I site of the vector. To construct pSRB01/pSRB02, the dCas9 fragment was amplified from pCRISPR-Cas9 using the primers dCas9-F/R and fused with the *ermE** promoter. The obtained fragment was ligated into pSR04 using EcoRI. The gRNA spacer sequences of the *bkdA1B1C1* and *bkdA2B2C2* promoters were designed using the primers bkd1-sgRNA-F2 and bkd2-sgRNA-F2. The corresponding sgRNA cassette was ligated into the Eco105I site of the vector. To construct pIB02, the *bkdA2B2C2* and *lipAB* genes were amplified from genomic DNA using the primers ermEp-bkd2-F/R, ermEp-lipA-F2/R2 and ermEp-lipB-F/R respectively. The fused fragment was ligated into the NdeI and EcoRV sites of vector pIJ8661. pMSBBAC1 was constructed by Eight Star Biotech (Wuhan, China), and the combinatorial expression fragment amplified by ermEp-bkd2-F2/R2 was ligated into pSOA01 to generate pSOA02.

Transformation of N. gerenzanensis *L70*

For the preparation of the donor *E. coli* cells, all recombinant plasmids were transferred into *E. coli* ET12567/

pUZ8002. An overnight suspension culture (200 μl) was inoculated in 20 ml of LB medium containing 50 μg ml^{-1} apramycin, 25 μg ml^{-1} chloramphenicol and 50 μg ml^{-1} kanamycin. After 3 − 4 h incubation at 37°C and 250 rpm, cultured *E. coli* with an optical density of 0.4 − 0.6 at 600 nm (OD600) were collected by centrifugation at 4000 *g* for 5 min, washed three times with sterile LB medium, and resuspended in 500 μl of LB medium. To prepare *N. gerenzanensis* mycelia, a 1 cm^2 agar piece from plate colonies cultured for 6 − 10 days was inoculated into 30 ml of YEME medium and cultured at 28°C and 220 rpm for 48 h. Then 1 ml of the mycelia was harvested by centrifugation at 4000 *g* for 5 min, washed three times with sterile LB medium, and resuspended in 500 μl of LB medium. Finally, about 10^9 donor *E. coli* cells were mixed with about 10^7 mycelium cells and spread on the plate with MS medium supplemented with 10 mM $MgCl_2$. After cocultivation at 28°C for 16 − 18 h, each plate was covered with 500 μl of sterile deionized water containing 1.5 mg apramycin and 0.75 mg nalidixic acid. Transformants were observed after 7−10 days and transferred into YMG plates with 50 μg ml^{-1} apramycin to select mutants.

Diagnostic PCR

Mycelia extracted from colonies on the screening plates were lysed by ultrasonication and harvested by centrifugation at 10 000 *g* for 5 min. The supernatant was then mixed with an equal volume of phenol-chloroform-isoamyl alcohol (25:24:1, pH = 8). Protein precipitates were removed by centrifugation at 10 000 *g* for 10 min. Equal volumes of isopropyl alcohol were added and incubated for 30 min to precipitate the gDNA. The gDNA samples were used as templates for diagnostic PCR, and the primers for diagnostic PCR are listed in Table S7.

Metabolites analysis

After 7 days of cultivation in YS medium, the culture was mixed with methanol in equal proportions and sonicated for 1 h to disrupt the cells. The sample was centrifuged at 10 000 *g* for 10 min. The supernatant was filtered through a 0.22 μm filter (Millipore, Billerica, MA, USA) for analysis. HPLC analysis of A40926 was performed on an Agilent 1260 infinity system (Agilent, San Diego, CA, USA) equipped with a DAD detector at 220 nm. The column used was an Agilent ZORBAX Eclipse Plus C18 (5 μm, 4.6 × 250 mm^2). Trifluoroacetic acid (0.1% in water) was mobile phase A and acetonitrile containing 0.1% trifluoroacetic acid was mobile phase B. For the analysis of A40926 production and composition, the chromatographic condition performed a linear gradient from 30% to 50% (v/v) B over 30 min and a subsequent isocratic stage of 90% B for 10 min at a constant flow rate of 1 ml min^{-1}. For the analysis of total metabolites, a linear gradient from 10% to 90% (v/v) B over 30 min and a subsequent isocratic stage of 90% B for 10 min at a constant flow rate of 1 ml min^{-1} was applied.

For the identification of A40926B0 and its derivatives in the sample, liquid chromatography-mass spectrometry (LC-MS) analysis was performed using the same parameters as those used for HPLC analysis. Electrospray ionisation (ESI)-MS was conducted on a Thermo Finnigan LCQ Deca XP MAX system, with the ESI source operating in positive ionization mode. The scan range was m/z 400−2000. Using an A40926B0 standard as a reference, the retention time of A40926A0, A40926A1, A40926B0, A40926B1, A40926C0, A40926C1, A40926D0 and A40926D1 was 11.092, 11.650, 14.510, 14.988, 17.759, 18.433, 21.325 and 21.946 min respectively (Fig. 4A, B and S5).

For the identification of metabolites in the different metabolic pathways, 1 ml extract solution (methanol: acetonitrile: water, 2: 2: 1) containing isotopically labelled internal standard mixture was added to the sample. The samples were sonicated for 20 min and centrifuged at 10 000 *g* for 20 min at 4°C. The resulting supernatant was transferred for analysis. LC-tandem MS (MS/MS) analysis were performed using a Vanquish ultra-HPLC system (Vanquish, Thermo Fisher Scientific) with an ultra-performance LC (UPLC) BEH Amide column (2.1 mm × 100 mm, 1.7 μm) coupled to a Q Exactive HFX mass spectrometer (Orbitrap MS, Thermo Fisher Scientific). The mobile phase consisted of 25 mM ammonium acetate and 25 ammonia hydroxide in water (pH = 9.75) (A) and acetonitrile (B). The QE HFX mass spectrometer was used to acquire MS/MS spectra in the information-dependent acquisition mode using Xcalibur acquisition software (Thermo Fisher Scientific). The ESI source was operated in both positive and negative ionization modes.

Quantitative RT-PCR

Mycelia of *N. gerenzanensis* L70 were washed twice with RNase-free TE buffer and total RNA extraction was performed using the EASYspin Plus bacteria RNA extract kit (Aidlab Biotech, Beijing, China) according to the manufacturer's guidelines. The RNA was treated with RNase-free DNase I (TaKaRa Bio, Shiga, Japan) to eliminate residual genomic DNA. After PCR validation, the RNA samples were reverse transcribed into cDNA using the PrimeScript™ 1st Strand cDNA Synthesis Kit (TaKaRa Bio) following the manufacturer's guidelines. Quantitative real-time PCR (qRT-PCR) was performed on a LightCycler 480 (Roche, Mannheim, Germany)

using TB Green™ Premix Ex Taq™ II (TaKaRa Bio) with the primers listed in Table S7 according to the manufacturer's guidelines. Fold changes in genes in different samples were quantified by normalizing to the expression level of *hrdB*.

RNA-seq analysis

All the RNA samples were prepared as above from mycelia cultured for 72 h. A total amount of 3 μg RNA per sample was used as input material for transcriptome sequencing. The preparations were sequenced on an Illumina Novaseq platform (Illumina, San Diego, CA, USA) and 150 bp paired-end reads were generated. HTSeq v0.6.1 was used to count the reads numbers mapped to each gene. Fragments per kilobase of transcript per million mapped reads (FPKM) were calculated to estimate gene expression levels.

Analysis of fatty acids

Mycelia cultured for 72 h were suspended in 6 ml of methanol containing 2% HCl and heated at 85°C for 2 h. Then 1 ml of 14% boron trifluoride in methanol was added to form fatty acid methyl esters (FAMEs) after heating at 100°C for 15 min. The methanolysate was evaporated to dryness and extracted with 1 ml n-hexane, which was injected onto a 7890B/7000C GC-MS system equipped with a 30 m × 0.25 mm × 0.25 μm HP-5MS column. Helium was used as the carrier gas at a constant flow rate of 1 ml min^{-1} and a split ratio of 20:1. The temperature was maintained at 50°C for 2 min, increased at a rate of 20°C min^{-1} to 150°C, 10°C min^{-1} to 200°C for 10 min, 2.5°C min^{-1} to 215°C for 8 min and 5°C min^{-1} to 270°C for 5 min. The mass spectrometer ion-source temperature was 250°C, and the scan range was 50–550 m/z.

Docking analysis of Dbv8 with acyl-CoAs

The crystal structure of acyltransferase in complex with decanoyl-CoA (Protein Data Bank code 4MFZ) was used as the template for docking of eight fatty acid-CoAs. The three-dimensional (3D) structure of the ligand was downloaded from PubChem, with hydrogen atoms and electric charges added. The energy of the ligand was optimized using the MMFF94 field. The UCSF Chimera molecular visualization program was used to prepare the ligands and receptors. Decanoyl-CoA in the eutectic structure was used as a reference ligand to define the combined pocket by removing water molecules and other ions. A docking grid box was then generated, and UCSF DOCK 6.9 was employed for docking. Each pose was extracted with the lowest binding energy and analysed using PyMOL.

Acknowledgements

This work was supported by the National Key Research and Development Program (grant number 2019YFA09005400) and key project from the National Natural Science Foundation of China (grant number 31730002).

Conflict of interest

The authors declare no competing interests.

Author contributions

T.Y. Xia and Y.Q. Li designed the study. T.Y. Xia conducted the experiments and wrote the manuscript. T.Y. Xia and X.A. Chen analysed the data. X.A. Chen, Y.Q. Liu, D H. Scharf, Q.W. Zhao and Y.Q. Li revised the manuscript. All authors read and approved the final manuscript.

References

Alt, S., Bernasconi, A., Sosio, M., Brunati, C., Donadio, S., and Maffioli, S.I. (2019) Toward single-peak dalbavancin analogs through biology and chemistry. *ACS Chem Biol* **14:** 356–360.

Bentley, G.J., Jiang, W., Guamán, L., Xiao, Y., and Zhang, F. (2016) Engineering *Escherichia coli* to produce branched-chain fatty acids in high percentages. *Metab Eng* **38:** 148–158.

Boucher, H.W., Wilcox, M., Talbot, G.H., Puttagunta, S., Das, A.F., and Dunne, M.W. (2014) Once-weekly dalbavancin versus daily conventional therapy for skin infection. *N Engl J Med* **370:** 2169–2179.

Cavaleri, M., Jabes, D., Henkel, T., Malabarba, A., Mosconi, G., Stogniew, M. & White, R.J. (2005) Methods of administering dalbavancin for treatment of bacterial infections. US patent US 200910298748 A1

Cho, J.S., Choi, K.R., Prabowo, C., Shin, J.H., Yang, D., Jang, J., and Lee, S.Y. (2017) CRISPR/Cas9-coupled recombineering for metabolic engineering of *Corynebacterium glutamicum*. *Metab Eng* **42:** 157–167.

Ebersbach, G., and Gerdes, K. (2005) Plasmid segregation mechanisms. *Annu Rev Genet* **39:** 453–479.

Galina, F., Galina, K., and Reynolds, K. A. (2002) Enzymes involved in fatty acid and polyketide biosynthesis in streptomyces glaucescens: role of FabH and FabD and their acyl carrier protein specificity. *Biochemistry* **41:** 10462–10471.

Gummerlich, N., Manderscheid, N., Rebets, Y., Myronovskyi, M., Gläser, L., Kuhl, M., *et al.* (2021) Engineering the precursor pool to modulate the production of pamamycins

in the heterologous host *S. albus* J1074. *Metab Eng* **67:** 11–18.

Herai, S., Hashimoto, Y., Higashibata, H., Maseda, H., Ikeda, H., Omura, S., and Kobayashi, M. (2004) Hyper-inducible expression system for streptomycetes. *Proc Natl Acad Sci USA* **101:** 14031–14035.

Hertweck, C. (2009) The biosynthetic logic of polyketide diversity. *Angew Chem Int Ed* **48:4688–4716.**

Hopwood, D.A., and Sherman, D.H. (1990) Molecular genetics of polyketides and its comparison to fatty acid biosynthesis. *Annu Rev Genet* **24:** 37–66.

Imre, A., Olasz, F., Kiss, J., and Nagy, B. (2006) A novel transposon-based method for elimination of large bacterial plasmids. *Plasmid* **55:** 235–241.

Jovetic, S., Feroggio, M., Marinelli, F., and Lancini, G. (2008) Factors influencing cell fatty acid composition and A40926 antibiotic complex production in *Nonomuraea* sp. ATCC 39727. *J Ind Microbiol Biotechnol* **35:** 1131–1138.

Kallscheuer, N., Vogt, M., Stenzel, A., Gätgens, J., Bott, M., and Marienhagen, J. (2016) Construction of a *Corynebacterium glutamicum* platform strain for the production of stilbenes and (2S)-flavanones. *Metab Eng* **38:** 47–55.

Kiatpapan, P., and Murooka, Y. (2002) Genetic manipulation system in propionibacteria. *J Biosci Bioeng* **93:** 1–8.

Koendjbiharie, J. G. (2015) Increasing production of 3-hydroxypropionic acid by modulating the activity of acetyl-CoA carboxylase 1 in Saccharomyces cerevisiae.

Kwong, S.M., Yeo, C., Suwanto, A., and Poh, C.L. (2000) Characterization of the endogenous plasmid from *Pseudomonas alcaligenes* NCIB 9867: DNA sequence and mechanism of transfer. *J Bacteriol* **182:** 81–90.

Leavitt, A., Chmelnitsky, I., Ofek, I., Carmeli, Y., and Navon-Venezia, S. (2010) Plasmid pKpQIL encoding KPC-3 and TEM-1 confers carbapenem resistance in an extremely drug-resistant epidemic *Klebsiella pneumoniae* strain. *J Antimicrob Chemother* **65:** 243–248.

Li, H., Wei, J., Dong, J., Li, Y., and Guan, W. (2020) Enhanced triacylglycerol metabolism contributes to efficient oil utilization and high production of salinomycin in *Streptomyces albus* ZD11. *Appl Environ Microbiol*, **86,** e00763–20.

Li, L., Zheng, G., Chen, J., Ge, M., Jiang, W., and Lu, Y. (2017) Multiplexed site-specific genome engineering for overproducing bioactive secondary metabolites in actinomycetes. *Metab Eng* **40:** 80–92.

Lu, C., Zhang, X., Jiang, M., and Bai, L. (2016) Enhanced salinomycin production by adjusting the supply of polyketide extender units in *Streptomyces albus*. *Metab Eng* **35:** 129–137.

Lyu, S.Y., Liu, Y.C., Chang, C.Y., Huang, C.J., Chiu, Y.H., Huang, C.M., *et al.* (2014) Multiple complexes of long aliphatic N-acyltransferases lead to synthesis of 2,6-diacylated/2-acyl-substituted glycopeptide antibiotics, effectively killing vancomycin-resistant enterococcus. *J Am Chem Soc* **136:** 10989–10995.

Marcone, G.L., Foulston, L., Binda, E., Marinelli, F., Bibb, M., and Beltrametti, F. (2010) Methods for the genetic manipulation of *Nonomuraea* sp. ATCC 39727. *J Ind Microbiol* **37:** 1097–1103.

Milke, L., and Marienhagen, J. (2020) Engineering intracellular malonyl-CoA availability in microbial hosts and its impact on polyketide and fatty acid synthesis. *Appl Microbiol Biotechnol* **104:** 6057–6065.

Netzker, T., Schroeckh, V., Gregory, M.A., Flak, M., and Brakhage, A.A. (2016) An Efficient method to generate gene deletion mutants of the rapamycin-producing bacterium *Streptomyces iranensis* HM 35. *Appl Environ Microbiol* **82:** 3481–3492.

Santos, C., Koffas, M., and Stephanopoulos, G. (2011) Optimization of a heterologous pathway for the production of flavonoids from glucose. *Metab Eng* **13:** 392–400.

Satoh, S., Ozaki, M., Matsumoto, S., Nabatame, T., Kaku, M., Shudo, T., Asayama, M., and Chohnan, S. (2020) Enhancement of fatty acid biosynthesis by exogenous acetyl-CoA carboxylase and pantothenate kinase in *Escherichia coli*. *Biotech Lett* **42:** 2595–2605.

Shuai, L., Chen, X.A., Mao, X.M., and Li, Y.Q. (2018) Regulatory and biosynthetic effects of the bkd gene clusters on the production of daptomycin and its analogs A21978C1–3. *J Ind Microbiol Biotechnol* **45:** 1–9.

Sofia, S., Sara, A., Stefano, D., and Margherita, S. (2010) A gene transfer system for the glycopeptide producer *Nonomuraea* sp. ATCC39727. *FEMS Microbiol Lett* **225:** 53–57.

Sosio, M., Canavesi, A., Stinchi, S., and Donadio, S. (2010) Improved production of A40926 by *Nonomuraea* sp. through deletion of a pathway-specific acetyltransferase. *Appl Microbiol Biotechnol* **87:** 1633–1638.

Sosio, M., Stinchi, S., Beltrametti, F., Lazzarini, A., and Donadio, S. (2003) The gene cluster for the biosynthesis of the glycopeptide antibiotic A40926 by *Nonomuraea* species. *Chem Biol* **10:** 541–549.

Stirrett, K., Denoya, C., and Westpheling, J. (2009) Branched-chain amino acid catabolism provides precursors for the Type II polyketide antibiotic, actinorhodin, via pathways that are nutrient dependent. *J Ind Microbiol Biotechnol* **36:** 129–137.

Strieker, M., and Dr, M.A.M. (2010) The structural diversity of acidic lipopeptide antibiotics. *ChemBioChem* **10:** 607–616.

Sun, N., Wang, Z.-B., Wu, H.-P., Mao, X.-M., and Li, Y.-Q. (2012) Construction of over-expression shuttle vectors in Streptomyces. *Ann Microbiol* **62:** 1541–1546.

Wan, L.D., Gek, N.B., and Seok, K.B. (2015) Increased valinomycin production in mutants of *Streptomyces* sp. M10 defective in bafilomycin biosynthesis and branched-chain α-keto acid dehydrogenase complex expression. *J Ind Microbiol Biotechnol* **42:** 1507–1517.

Wang, K., Zhao, Q.-W., Liu, Y.-F., Sun, C.-F., Chen, X.-A., Burchmore, R., *et al.* (2019) Multi-layer controls of cas9 activity coupled with ATP synthase over-expression for efficient genome editing in streptomyces. *Front Bioeng Biotechnol* **7:** 304.

Wang, W., Yang, T., Li, Y., Li, S., Yin, S., Styles, K., *et al.* (2016) Development of a synthetic oxytetracycline-inducible expression system for streptomycetes using de novo characterized genetic parts. *ACS Synth Biol* **5:** 765–773.

Wang, X.K., and Jin, J.L. (2014) Crucial factor for increasing the conjugation frequency in Streptomyces netropsis SD-07 and other strains. *FEMS Microbiol Lett* **357,** 99–103.

Wu, Q., Zhi, Y., and Xu, Y. (2019) Systematically engineering the biosynthesis of a green biosurfactant surfactin by *Bacillus subtilis* 168. *Metab Eng* **52:** 87–97.

Xi, L., Yang, Y., Wen, L., Hao, Z., and Shang, G. (2016) Pseudomonas putida KT2440 markerless gene deletion using a combination of λ Red recombineering and Cre/loxP site-specific recombination. *FEMS Microbiol Lett* **363:** fnw014.

Xie, S., Shen, B., Zhang, C., Huang, X., and Zhang, Y. (2014) sgRNAcas9: a software package for designing CRISPR sgRNA and evaluating potential off-target cleavage sites. *PLoS One* **9:** e100448.

Yi, X., Li, S., Liang, M., Zhang, G., and Zhang, C. (2010) Genetic manipulation system for tiacumicin producer *Dactylosporangium aurantiacum* NRRL 18085. *Acta Microbiol Sinica* **50:** 1014–1022.

Zabala, D., Braa, A.F., Flórez, A., Salas, J.A., and Méndez, C. (2013) Engineering precursor metabolite pools for increasing production of antitumor mithramycins in *Streptomyces argillaceus*. *Metab Eng* **20:** 187–197.

Zaman, M.A., Pasha, M.H., and Akhter, M.Z. (2011) Plasmid curing of escherichia coli cells with ethidium bromide, sodium dodecyl sulfate and acridine orange. *J Microbiol* **27:** 28–31.

Zerilli, L.F., Edwards, D., Borghi, A., Gallo, G.G., Selva, E., Denaro, M., and Lancini, G.C. (2010) Determination of the acyl moieties of the antibiotic complex A40926 and their relation with the membrane lipids of the producer strain. *Rapid Commun Mass Spectrometry Rcm* **6:** 109–114.

Zhanel, G.G., Calic, D., Schweizer, F., Zelenitsky, S., Adam, H., Lagacé-Wiens, P., *et al*. (2010) New lipoglycopeptides: a comparative review of dalbavancin, oritavancin and telavancin. *Drugs* **70:** 859–886.

Supporting information

Additional supporting information may be found online in the Supporting Information section at the end of the article.

Fig. S1. Comparison of morphological phenotype and A40926B0 production in *Nonomuraea* sp. ATCC 39727 and *N. gerenzanensis* L70.

Fig. S2. Evaluation of the conjugation efficiency (A) and gene-editing efficiency (B) of plasmid tools based on the traditional genetic strategies.

Fig. S3. Growth status of the corresponding mutants on the MS plates.

Fig. S4. Nucleotide sequence alignment of NGR70 in NCBI database.

Fig. S5. Growth status of the corresponding mutants on the MS plates.

Fig. S6. MS and UV spectra of A40926 components.

Fig. S7. Production analysis of each component corresponding to the number of A40926 complex (**Fig. 4B**) by HPLC in IPB-2 compared with that in L70.

Fig. S8. Relative levels of the identified metabolites in the different metabolic pathways.

Fig. S9. Production analysis of each component corresponding to the number of A40926 complex (**Fig. 4B**) by HPLC in IPB-4 compared with that in IPB-3.

Fig. S10. Amino acid alignments of partial sequence of BCDH complex in *N. gerenzanensis* L70 and other actinomycetes.

Fig. S11. Plasmid map of pSRB01 based on the erCRISPR-dCas9 system.

Fig. S12. The relative expression of *bkdA1B1C1* and *bkdA2B2C2* in IPB-4 and IPB-5.

Fig. S13. MS spectra of FAMEs for *N. gerenzanensis* cell fatty acids.

Fig. S14. Comparison of A40926B0 production with supplementation of sodium isobutyrate at different concentrations.

Fig. S15. Production analysis of each component corresponding to the number of A40926 complex (**Fig. 4B**) by HPLC in IPB-7 supplemented with 10 mM sodium isobutyrate compared with that in IPB-7.

Fig. S16. Molecular docking of fatty acyl-CoAs with the acyltransferase Dbv8 and evaluation of Dbv8 substrate affinity for fatty acyl-CoAs.

Fig. S17. Validation of two extra copies of the dbv gene cluster.

Fig. S18. HPLC analysis of A40926 components in fermentation broths.

Table S1. Proposed functions of ORFs in P1.

Table S2. Proposed functions of ORFs in P2.

Table S3. Prediction of possible secondary metabolites of gene clusters in *Nonomuraea gerenzanensis L70* and transcriptional levels of the core synthases

Table S4. Proposed functions of ORFs in the *vpk*-gene cluster.

Table S5. Strains and plasmids used in this study.

Table S6. List of protospacers and PAM sequences of each target locus in this study.

Table S7. Oligonucleotides used in this study.

